

Article

Analysis and Optimization of the Coordinated Multi-VSG Sources

Xiangwu Yan ¹, Aazim Rasool ^{1,2,*} , Farukh Abbas ³ , Haaris Rasool ⁴ and Hongxia Guo ²

¹ Department of Electrical Engineering, North China Electric Power University, Baoding 071003, China; xiangwuy@ncepu.edu.cn

² Goldwind Science and Technology, Co. Ltd., Beijing 100176, China; guohongxia@goldwind.com.cn

³ School of Electronics, Information and Electrical Engineering, Shanghai Jiao Tong University, Shanghai 200240, China; abbas1990@sjtu.edu.cn

⁴ Electrical Engineering and Power Electronics Department, Vrije Universiteit Brussel; Boulevard de la Plaine 2, 1050 Ixelles, Belgium; haaris.rasool@vub.ac.be

* Correspondence: a.rasool@ncepu.edu.cn; Tel.: +86-15611897523

Received: 18 November 2018; Accepted: 21 December 2018; Published: 26 December 2018



Abstract: The penetration of renewable energy sources (RES) into a grid via inverters causes a stability issue due to the absence of an inertia. A virtual synchronous generator (VSG) is designed to provide an artificial inertia and droop control to the grid-connected inverters. The different power ratings of multiple VSGs create complications in the coordination due to unequal droop or damping coefficient 'D'. The dependency of a factor 'D' on $P - \omega$ droop control under static state and a damping behavior during power oscillation under dynamic state is analyzed by considering three cases on multi-VSGs microgrid system and the equivalent equations of $P - \omega$ droop control are derived for all three cases to see the effect of a load on the overall system's frequency. A master–slave configuration of a VSG is proposed to deliver maximum power during static state, but provides $P - \omega$ control during the dynamic state. Simulation results verify the improvement introduced by the proposed VSG control.

Keywords: virtual synchronous generator; parallel VSGs; droop control; optimization; multiple VSGs coordination; island microgrid

1. Introduction

The high penetration of renewable energy systems (e.g., wind and solar) have a negligible inertia as compared to the conventional synchronous generator. It is a serious challenge for the future grid as the penetration of RES is decreasing the overall inertia of a grid and it is severely affecting the reliability of a grid. The lower inertia of a grid causes a higher rate of change of frequency (RCF) that brings the frequency of a source to its nadir frequency (minimum frequency) at which the RES source tripped off. Consequently, the overall load on a generation rises and it further trips off the other source. In a severe condition, a grid shutdown could lead to a blackout condition. Therefore, robust control is required to stabilize the power system more than ever before. RESs (e.g., wind, solar) usually operate at their maximum generating power, with an aim to utilize the maximum natural resources. For this purpose, maximum power point tracking (MPPT) technique has been utilized [1]; this in turn significantly reduces the power margin that is required for any transition or disturbance condition. A microgrid provides a solution to this drawback of RESs by accumulating a number of RES-distributed generators (DGs), along with the energy storage system (ESS) and the loads. There are various schemes of a microgrid, however, the best configuration contains RESs, ESSs (fast, and slow both), nonrenewable sources and the loads.

Many controls are available to operate microgrids, though every control has its own advantages and drawbacks. In a conventional power system, the main source of electricity is the synchronous

generator. The synchronous generator has inherent droop and inertia controls that critically helps in stabilizing the power system by damping the effect of dynamic transition at the time of any fault or disturbance. When the number of synchronous generators is connected with a grid, then each SG follows the decentralized control (droop) to contribute its share. Hence, implementing the characteristic of a synchronous generator in an inverter control can be considered as a reasonable solution in terms of sharing active and reactive power among DGs of a microgrid. The implementation of droop control in the inverter and the advancement in droop control to operate the multiple inverters connecting in parallel is presented in [2,3]. There are several droop control mechanism such as $P - f$, $Q - V$, $P - V$ [2–5]. The hierarchical control structure in case of a communication link failure in an islanded AC microgrid is presented in [6].

The recent control of inverter that has almost all the characteristics of a synchronous generator is known as a virtual synchronous generator (VSG). In droop control, only the droop behavior of SG is present, whereas, in VSG, virtual rotation inertia also exists in its control [7,8]. The alternative controls of VSG are presented in different research papers: the virtual synchronous machine (VSM) in [9], virtual synchronous machine (VISMA) in [10] and the synchronverter in [11]. However, the drawback of VSG over SG is a lack of overload capability to ride through large oscillations and the inappropriate sharing of active and reactive transient power among VSGs that can critically cause the oscillation in active power during a disturbance [12]. In recent research, a number of improvements in a VSG control and its applications have been introduced [13–15]. The problem of overload capacity in VSG can be overcome by using energy storage—a number of solutions are presented in the literature to solve an uneven sharing of power and the proper coordination of VSGs in a microgrid. The performance of a system is enhanced by using VSG control technique based on the Hamilton approach is presented in [16]. The alternate moment of inertia is a technique that uses different values of inertia coefficient during a dynamic state to dampen the oscillation of a system in less time [17], the output power oscillation is solved by properly increasing a damping ratio after observing the derivative of voltage, active and reactive power, and the phase difference in [18]; the enhancement of dynamic response of an inverter by using a smaller value of inertia is presented in [19]; the virtual stator reactance technique is used to reduce the power oscillation in [12]; sharing the transient load by using generator emulation method is presented in [20]; the stabilization through bouncy control by introducing alternative emergency gain during transition state is presented in [21]. These are a few techniques to resolve the power oscillation problem. However, there is still a necessity to further improve the coordination among different VSGs within a microgrid and with other microgrids. The analysis techniques to observe the stability of a power system are presented in [21–24]. The coordination control for multiple DG units to improve transient performance is presented in [25].

In the view of the above-mentioned issue, this paper is presenting the correlation and the dependency of different parameters of VSG on its fellow VSG. The in-depth analysis is performed for the static characteristic (droop) and the dynamic characteristic (damping) due to a droop coefficient. It is worth noticing that the droop does not only contribute in a static state, but it also participates in the dynamic state along with an inertia. A novel master–slave VSG control configuration is also introduced by utilizing the above relationship between VSGs to operate RESs at the maximum power without compromising the stabilizing characteristic of VSG control. The load analysis, rate of change of frequency analysis and fault analysis are performed in four cases.

2. Operation of VSG

Virtual synchronous generator (VSG) is an inverter control that mimics the operation of a synchronous generator due to its inherent inertia and droop control.

The block diagram of VSG control is shown in Figure 1. The control is designed in dq-axis. The reference rotational frequency of dq-axis is ω_g in an isolated system, while in a grid-connected

VSG, it adopts the rotational frequency of the grid. The double voltage current controller is used in this VSG control system. The basic swing equation for VSG control is in Equation (1)

$$J \frac{\partial(\omega - \omega_g)}{\partial t} = \frac{P_{ref} - P}{\omega} - D(\omega_g - \omega) \tag{1}$$

$$E_{ref} = E + I(r_a + jx_a) \tag{2}$$

where P_{ref} is the reference power, P_e is the measured output power, D is the droop coefficient, J is the virtual inertia, ω is the virtual angular frequency of VSG and ω_g is the angular frequency of the grid or power common coupling (PCC). E is the excitation electromotive force and I is the stator current. r_a and x_a are a resistance and a reactance of stator winding in the synchronous generator.

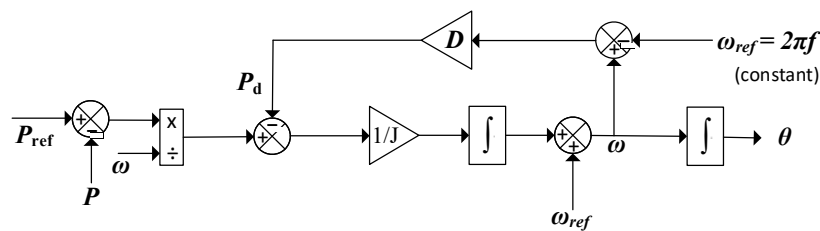


Figure 1. Basic VSG control diagram.

The reactive power and voltage droop control is shown in Figure 2. Equations (3) and (4) show the $P - \omega$ and the $Q - V$ droop control D_p and D_q are the droop coefficients of $P - \omega$ and $Q - V$ respectively.

$$\omega = \omega_{ref} - D_p(P - P_{ref}) \tag{3}$$

$$u = u_{ref} - D_q(Q - Q_{ref}) \tag{4}$$

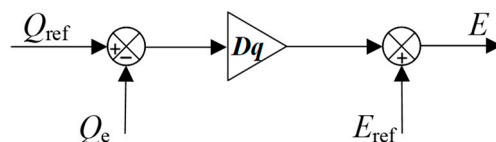


Figure 2. Voltage and reactive power control of VSG.

The overall control of each VSG is shown in Figure 3. Three phase voltage and current from a terminal of a VSG; after LC filter and a grid are measured. The control is designed in dq-axis, therefore, the measured parameters are first transformed from abc-axis to dq0-axis by using the Park’s transformation. The active and reactive power is calculated in (5), and frequency is detected via phase locked loop (PLL) [26]. ‘ P_{ref} ’ is the reference power of VSG control that has a constant value in this research. VSG control decides the excitation voltage and phase angle by observing the acquired system’s parameter values. By using V and θ , three-phase voltage in abc-axis is generated, which is then transformed to dq0-axis; before going to voltage and current loop control. The reference voltage in dq0-axis is transformed into abc-axis. Pulse width modulator (PWM) generates a square signal for the inverter to produce the reference AC voltage

$$\begin{aligned} P &= \frac{3}{2}(V_d I_d + V_q I_q) \\ Q &= \frac{3}{2}(V_q I_d - V_d I_q) \end{aligned} \tag{5}$$

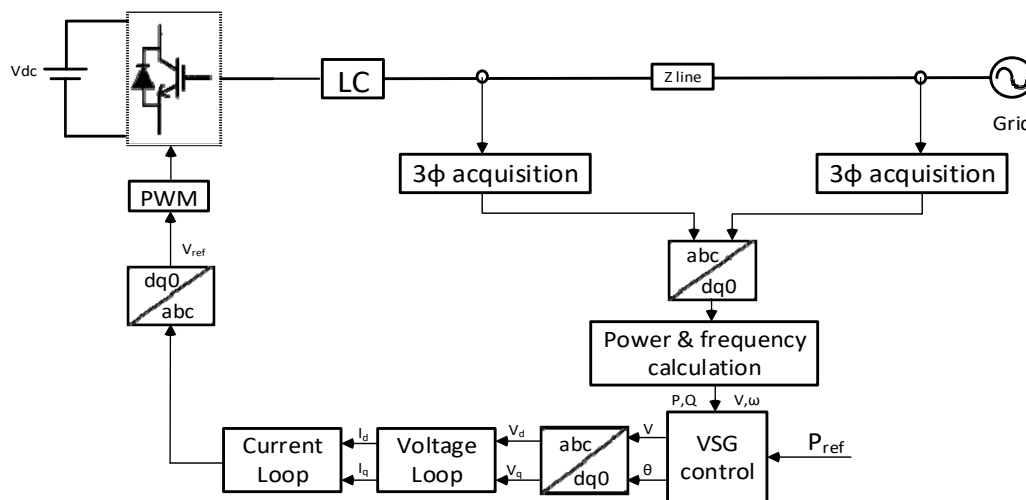


Figure 3. Overall control of VSG connected grid.

3. Effective Droop Control of Multiple-VSG System

A classical $P - \omega$ droop control functions such that an increase in a load causes a decrease in the rotational speed of a machine. The virtual synchronous generator has no rotating part so the angular frequency is considered to mimic the effect of a rotational speed in the synchronous generator. VSG operates at its reference frequency when a delivering power from the VSG is equal to its reference power. When the frequency is 50 Hz then an angular frequency is $2\pi f$ ($100\pi = 314.156$ Hz/s), the reference frequency. When a delivering power through VSG is less than the reference power, then the frequency is slightly higher than the reference frequency and that frequency is calculated through a droop controller.

3.1. The Significance of No-Load Angular Frequency in Load Sharing

No-load angular frequency has a substantial role in power sharing of a load for different powers rating and droop coefficients of multiple-VSG systems. A difference in no-load angular frequencies of two VSGs defines an offset (starting) power of one VSG even before a load sharing is initialized.

Multiple VSGs with different power ratings, and droop coefficient; having same reference frequency at 314.156 Hz/s are considered for the analysis. The load sharing is basically a static response of a VSG control, therefore the dynamic characteristic of the swing equation, as in (1) is eliminated to elaborate the static behavior of VSG. The static characteristic of swing equation is $P - \omega$ droop control, it can be expressed as,

$$\begin{aligned} slope &= \frac{1}{D} = \frac{\Delta\omega}{\Delta P} \times \omega^* = \frac{\omega - \omega_{ref}}{P_e - P_{ref}} \times \omega^* \\ \Rightarrow \omega &= \frac{|P_e - P_{ref}|}{D} \times \frac{1}{\omega^*} + \omega_{ref} \end{aligned} \tag{6}$$

A no-load frequency is calculated from the above equation by considering the power utilization at a load is zero ($P_e = 0$).

$$\omega_{nl} = \frac{P_{ref}}{D} \times \frac{1}{\omega^*} + \omega_{ref} \tag{7}$$

It can be observed from Equation (7) that ω_{nl} is dependent on a reference power of VSG. For the same droop coefficient, the higher reference power will have more no-load frequency; consequently, the offset power will be higher. The no-load frequencies for different parameters of VSG sources are displayed in Table 1.

Table 1. No-Load Frequency of Different VSGs.

P_{ref}	D	$\Delta\omega^m$ (Hz/s)	ω_{nl} (Hz/s)
15 kW	40	1.1936	315.35
10 kW	40	0.7957	314.95
7.5 kW	40	0.5968	314.75
7.5 kW	25	0.9549	315.11
7.5 kW	15	1.5915	315.74

The possible no-load angular frequency sequences of three VSGs connected in parallel are displayed in Figure 4. Out of them, only three highlighted cases are considered for the evaluation of a droop control as shown in Table 2.

Table 2. The Regional Conditions of Different Cases.

Cases	Condition	Region 1	Region 2	Region 3
Case I	$\omega_{nl}^1 > \omega_{nl}^2 > \omega_{nl}^3$	V-1	V-1, 2	V-1, 2, 3
Case II	$\omega_{nl}^1 > \omega_{nl}^3 > \omega_{nl}^2$	V-1	V-1, 3	V-1, 2, 3
Case III	$\omega_{nl}^3 > \omega_{nl}^1 > \omega_{nl}^2$	V-3	V-3, 1	V-1, 2, 3

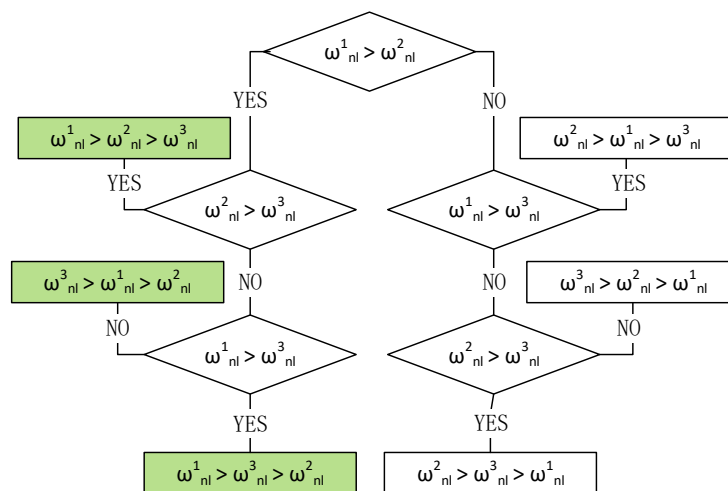


Figure 4. Possible sequences of three VSG sources w.r.t. no-load frequency.

3.2. Load Sharing Criteria

The load sharing criteria for three systems of multiple VSG sources is considered. The percentage of load distribution among multiple sources of different power ratings and droop coefficients is not the same. The droop control between two VSGs is only effective when a frequency is lower than the no-load frequencies of both VSGs. The equation of power sharing among three VSGs for a total load is represented in Equation (8) as,

$$P_l = P_1^t + P_2^t + P_3^t \tag{8}$$

The term ΔP_x^t is a total power contribution of a VSG; x is a number of VSGs. P_l is a total load of a system. The regions are defined on the basis of the difference in no-load angular frequency of VSG sources.

3.2.1. Case I

In a Case I, three VSG sources of different power ratings with a similar droop coefficient is considered to analyze the total power sharing by each VSG source and the overall effective $P - \omega$ droop control of three VSG sources as shown in Figure 5.

The power contribution in each region is represented as,

Region 1: In region 1, the only effective source is VSG-1. The power of VSG-1 at region 1 is represented as ΔP_1^{R1} and it can be expressed in terms of droop coefficient and angular frequency in (9).

$$\Delta P_m^{R1} = \Delta P_1^{R1} = \omega D_1 \Delta \omega_a \tag{9}$$

where, $\Delta \omega_a = \omega_{nl}^1 - \omega_{nl}^2$.

Region 2: In region 2, VSG-1 and VSG-2 are effective. The maximum available power in region 2 is a sum of ΔP_1^{R2} and ΔP_2^{R2} in Equation (10)

$$\Delta P_m^{R2} = \Delta P_1^{R2} + \Delta P_2^{R2} = (D_1 \Delta \omega_b + D_2 \Delta \omega_b) \omega \tag{10}$$

where, $\Delta \omega_b = \omega_{nl}^2 - \omega_{nl}^3$.

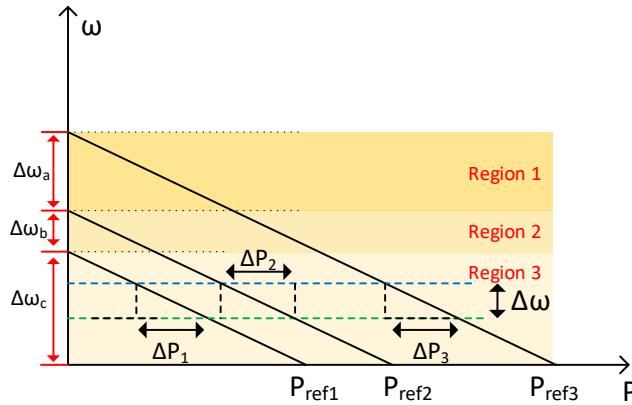


Figure 5. Regional Power Contribution Case I.

Region 3: In region 3, all three VSGs are available to contribute to load sharing. The maximum available power in region 3 is a sum of ΔP_1^{R3} , ΔP_2^{R3} and ΔP_3^{R3} in Equation (11)

$$\Delta P_m^{R3} = \Delta P_1^{R3} + \Delta P_2^{R3} + \Delta P_3^{R3} = (D_1 \Delta \omega_c + D_2 \Delta \omega_c + D_3 \Delta \omega_c) \omega \tag{11}$$

where $\Delta \omega_c$ is the maximum available change in angular frequency for three VSGs and it can be represented as, $\Delta \omega_c = \omega_{nl}^3 - \omega_{ref}$.

When a system is operated in region 3 then the maximum power of region 1 and region 2 is added as an offset power for VSG-1 and VSG-2. The change in load in region 3 produces an effect of equivalent droop in which all three VSG are operated with $P - \omega$ droop control. A detailed expression of Equation (8) is calculated from Equations (12)–(14) in (15).

$$P_1^{t-1} = \omega D_1 (\Delta \omega_a + \Delta \omega_b + \Delta \omega_c^{o-1}) \tag{12}$$

$$P_2^{t-1} = \omega D_2 (\Delta \omega_b + \Delta \omega_c^{o-1}) \tag{13}$$

$$P_3^{t-1} = \omega D_3 (\Delta \omega_c^{o-1}) \tag{14}$$

Equation (15) shows a load power sharing in terms of VSG power sources and Equation (16) shows a load sharing in terms of regions.

$$P_l = \omega D_1 (\Delta \omega_a + \Delta \omega_b + \Delta \omega_c^o) + \omega D_2 (\Delta \omega_b + \Delta \omega_c^o) + \omega D_3 (\Delta \omega_c^o) \tag{15}$$

$$P_l = \omega (D_1 \Delta \omega_a + (D_1 + D_2) \Delta \omega_b + (D_1 + D_2 + D_3) \Delta \omega_c^o) \tag{16}$$

where, $\Delta\omega_c^o = \omega_{nl}^3 - \omega^o$ and ω^o is an operating angular frequency of a system. The equation of change in load and power sharing among three VSG system at this point is in Equation (17).

$$\Delta P_l = \Delta P_1 + \Delta P_2 + \Delta P_3 \tag{17}$$

$\Delta P_l, \Delta P_1 = \omega D_1 \Delta\omega, \Delta P_2 = \omega D_2 \Delta\omega$ and $\Delta P_3 = \omega D_3 \Delta\omega$ are the instantaneous change in a power of load, VSG-1, VSG-2 and VSG-3 respectively. The equation of the actual load sharing among multiple VSG source is derived in Equations (18) and (19).

$$P_l + \Delta P_l = (P_1^t + \Delta P_1) + (P_2^t + \Delta P_2) + (P_3^t + \Delta P_3) \tag{18}$$

$$P_l + \Delta P_l = \omega \left(\begin{array}{l} D_1 \Delta\omega_a + (D_1 + D_2) \Delta\omega_b + \\ (D_1 + D_2 + D_3) (\Delta\omega_c^o + \Delta\omega) \end{array} \right) \tag{19}$$

3.2.2. Case II

In a Case II, three VSG sources of different power ratings with different droop coefficients are considered to analyze a total power sharing by each VSG source and the overall effective $P - \omega$ droop control of three VSG sources as shown in Figure 6. In this case, the droop coefficient of VSG-3 is set such that a no-load frequency is between the no-load frequency of VSG-1 and VSG-2. The load sharing equations of Case II are in Equations (20)–(23).

$$P_l^2 = \omega(D_1 \Delta\omega_a + (D_1 + D_3) \Delta\omega_b + (D_1 + D_2 + D_3) \Delta\omega_c^o) \tag{20}$$

$$P_1^{t-2} = \omega D_1 (\Delta\omega_a + \Delta\omega_b + \Delta\omega_c^{o-2}) \tag{21}$$

$$P_2^{t-2} = \omega D_3 (\Delta\omega_c^{o-2}) \tag{22}$$

$$P_3^{t-2} = \omega D_2 (\Delta\omega_b^2 + \Delta\omega_c^{o-2}) \tag{23}$$

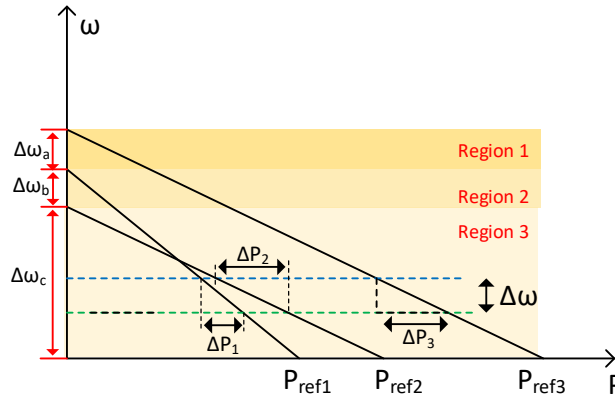


Figure 6. Regional Power Contribution Case II.

3.2.3. Case III

In a Case III, VSG-3 is introduced with a different droop coefficient so that the no-load frequency of VSG-3 is the highest among all sources as shown in Figure 7. The load sharing for each VSG source can be calculated from Equations (24)–(27).

$$P_l^3 = \omega(D_3 \Delta\omega_a + (D_1 + D_3) \Delta\omega_b + (D_1 + D_2 + D_3) \Delta\omega_c^o) \tag{24}$$

$$P_1^{t-3} = \omega D_1 (\Delta\omega_b^3 + \Delta\omega_c^{o-3}) \tag{25}$$

$$P_2^{t-3} = \omega D_2 (\Delta\omega_c^{o-3}) \tag{26}$$

$$P_3^{t-3} = \omega D_3(\Delta\omega_a^3 + \Delta\omega_b^3 + \Delta\omega_c^0) \tag{27}$$

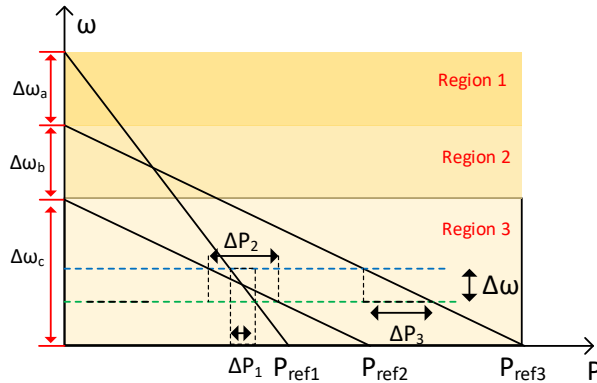


Figure 7. Regional Power Contribution Case III.

3.3. P – ω Control for Equivalent Droop

The variation of frequency on increase in load for three different cases is discussed. The operating frequency of a system for load ‘P_l’ is calculated for case I, II and III by rearranging Equations (16), (17) & (24) into (28), (29) & (30) respectively.

$$\omega^{o-1} = \omega_{nl}^3 - \frac{1}{D_{eq}^1} \left(\frac{P_l}{\omega} - D_1 \Delta\omega_a^1 - (D_1 + D_2) \Delta\omega_b^1 \right) \tag{28}$$

$$\omega^{o-2} = \omega_{nl}^2 - \frac{1}{D_{eq}^2} \left(\frac{P_l}{\omega} - D_1 \Delta\omega_a^2 - (D_1 + D_3) \Delta\omega_b^2 \right) \tag{29}$$

$$\omega^{o-3} = \omega_{nl}^2 - \frac{1}{D_{eq}^3} \left(\frac{P_l}{\omega} - D_3 \Delta\omega_a^3 - (D_1 + D_3) \Delta\omega_b^3 \right) \tag{30}$$

Case I: $\Delta\omega_a^1 = \omega_{nl}^1 - \omega_{nl}^2 = 0.4, \Delta\omega_b^1 = \omega_{nl}^1 - \omega_{nl}^2 = 0.2, \omega_{nl}^3 = 314.75, \omega^{o-1} = 314.48, \Delta\omega_c^{o-1} = 0.27$

Case II: $\Delta\omega_a^2 = \omega_{nl}^1 - \omega_{nl}^3 = 0.24, \Delta\omega_b^2 = \omega_{nl}^2 - \omega_{nl}^3 = 0.16, \omega_{nl}^2 = 314.95, \omega^{o-2} = 314.53, \Delta\omega_c^{o-2} = 0.42$

Case III: $\Delta\omega_a^3 = \omega_{nl}^3 - \omega_{nl}^1 = 0.39, \Delta\omega_b^3 = \omega_{nl}^3 - \omega_{nl}^2 = 0.4, \omega_{nl}^2 = 314.95, \omega^{o-3} = 314.57, \Delta\omega_c^{o-3} = 0.38$

3.4. Dynamic Response of Damping Coefficient

The droop coefficient and damping coefficient are the two characteristics of a coefficient ‘D’. The droop coefficient is referred with the static response of multiple VSG systems, whereas damping coefficient ensures the dynamic response. The correlation between multiple VSGs is built for the better understanding to differentiate its effects on the static and dynamic state. The dynamic behavior of a VSG due to a damping coefficient is assessed by omitting the effects of an inertia from a swing Equation (1) i.e., $J = 0$

$$D\omega(\delta\omega) = \delta P \Rightarrow \delta\omega = \frac{\delta P}{D\omega} \tag{31}$$

The derivative of the change in frequency is calculated by taking a derivative of Equation (31).

$$\dot{\delta\omega} = \frac{1}{D\omega} \dot{\delta P} \tag{32}$$

The damping coefficient D is inversely proportional to a derivative of angular frequency $\dot{\delta\omega}$. Hence, the decrease in the value of a damping coefficient causing an increase in a rate of $\dot{\delta\omega}$.

$$\dot{\delta\omega} \propto \frac{1}{D} \tag{33}$$

3.5. Power Percentage

The power sharing for among different VSG sources is calculated from a static characteristic of swing equation by considering equivalent droop coefficient and total power of a load.

$$\frac{1}{D_{eq}} = \frac{\Delta\omega}{\Delta P_1 + \Delta P_2 + \Delta P_3} \times \omega^* \tag{34}$$

$$D_{eq} = D_1 + D_2 + D_3 \tag{35}$$

The equivalent droop coefficient of three VSGs in a region 3 is a sum of all three droop coefficients. The percentage of change in power sharing is calculated from a droop coefficient. The terms y_1, y_2 & y_3 are the values of a proportion of a load division. The percentage of these terms can be calculated by multiplying them with 100 i.e., $y\% = y \times 100$.

$$y_1 = \frac{\Delta P_1}{\Delta P_t} = \frac{D_1}{D_{eq}}, y_2 = \frac{\Delta P_2}{\Delta P_t} = \frac{D_2}{D_{eq}}, y_3 = \frac{\Delta P_3}{\Delta P_t} = \frac{D_3}{D_{eq}} \tag{36}$$

3.6. Rate of Change of Frequency (RCF)

The increase in the penetration of renewable energy sources is causing a low inertia in a power grid. The coordination between multiple sources is quite essential than ever before. It is presumed in a literature that a rate of change of frequency (RCF) of multiple sources should be the same for a dynamic response matching. The RCF analysis of three sources for each case is considered to observe matching between sources.

4. Master-Slave Configuration of VSG

A master-slave control is introduced to obtain the maximum power of renewable energy source by using VSG control. The idea is to use the inertia and instant droop characteristic of VSG control during dynamic state while delivering a rated power to a microgrid system. It is configured such that it follows the operating (instant) angular frequency as a reference angular frequency to maintain its reference power as shown in Figure 8. VSG acts as an isochronous generator during static state and changes its behavior to the synchronous generator during dynamic state, therefore, the damping characteristic of VSG is always present to reduce the oscillation, however, the droop control during static condition is not operational. ω_o is the operating angular frequency of a system, therefore, the reference angular frequency is a variable term.

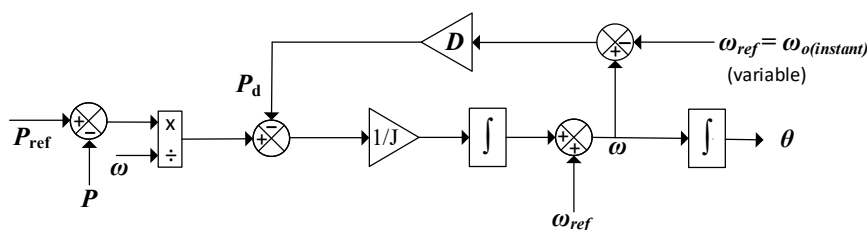


Figure 8. Master-slave configuration of VSG control.

Assuming an island microgrid system that has a similar condition of power and droop coefficient, but there is a dissimilarity in the reference frequency ' ω_{ref} ' of VSG-3, which is set to the instant angular

frequency of a grid. In this case, VSG-3 is contributed its maximum power all the time, whereas the droop control of VSG-1 and VSG-2 controls the overall $P - \omega$ droop control of the multi-VSG system. It doesn't matter whether the system's angular frequency is at the line (i) or at the line (ii) in Figure 9, the maximum power is delivered from VSG-3. It can be concluded that the droop control of VSG-3 has become insignificant to the system; except a small contribution at the time of dynamic state. The control equation of master-slave VSG control can be written as in (37).

$$J\omega \frac{\partial(\omega - \omega_0)}{\partial t} = (P_{ref} - P) - D\omega(\omega - \omega_0) \tag{37}$$

Here, ω_0 is an instant frequency of a system or a grid frequency and it is varying on the change in load (stand-alone microgrid), therefore, VSG-3 remains at its maximum power all the time. VSG-1 and VSG-2 are following an equivalent droop of two VSG sourced multi-VSG system and the reference frequency of both VSGs are 314.156 Hz/s ($f = 50$ Hz). The comparison of master-slave VSG (MS-VSG) and simple VSG control is presented in Table 3.

Table 3. Comparison of MS-VSG and Simple VSG control.

Parameter	MS-VSG (Proposed)	Simple VSG
ω_{ref}	Variable frequency	Fixed frequency
Inertia	Yes	Yes
Damping	Yes	Yes
Power deliver	Ref. power at any ω	Ref. power at ω_{ref} (100π)
$P - \omega$ droop	Only Dynamic state	Both Static and Dynamic state
$Q - V$ droop	Yes	Yes
Dependency of factor 'D'	Damping	Droop and damping both

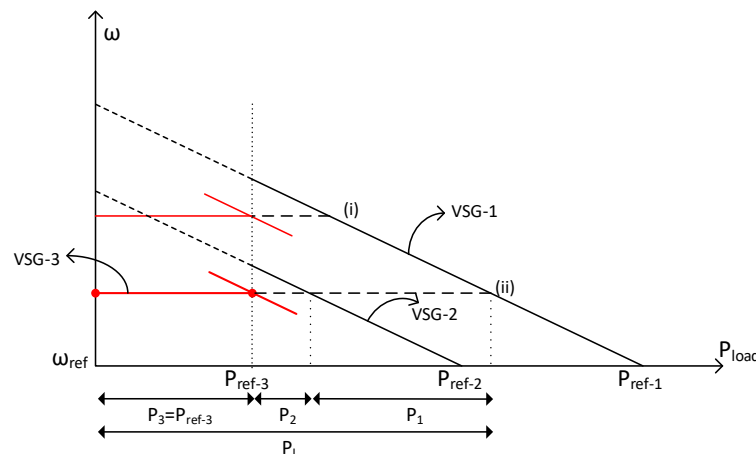


Figure 9. $P - \omega$ droop curve for master-slave configuration.

5. Island Microgrid of Multiple VSG Sources

The island microgrid of three VSG sources is designed to observe the performance of VSG-3 for different parameters and controls as shown in Figure 10. The power ratings of three VSGs are 15 kW, 10 kW and 7.5 kW for VSG-1, VSG-2 and VSG-3, respectively. The load of 20 kW and 10 kW is added at the start and 0.5 sec respectively. The DC supply of 800 V is used at the DC side of each source and the operating frequency is 50 Hz.

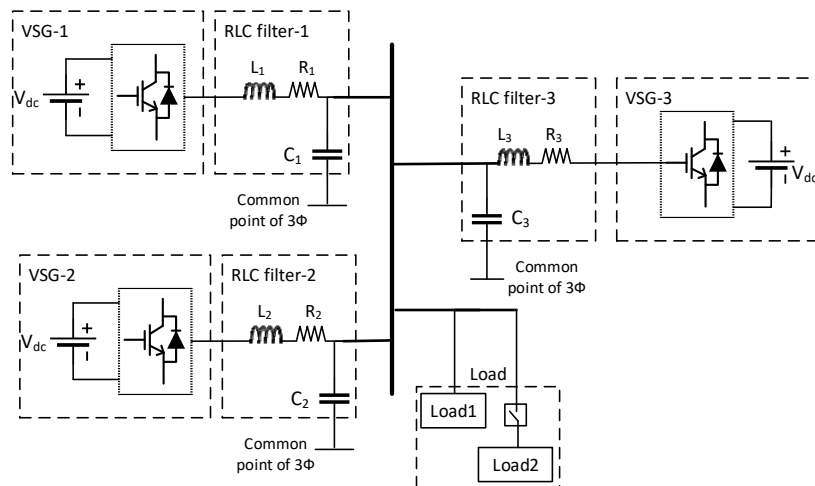


Figure 10. Island microgrid of a multiple-VSG system.

LC filter is designed by using the formula in Equation (38). We have chosen a damping factor $D_p = 40$, which means that a frequency drop of 0.4%, 0.25%, and 0.2% cause the power to increase by 100% for 15 k, 10 k and 7.5 k respectively. The detailed parameters of the multi-VSG system are shown in Table 4.

$$L \geq \frac{1}{2\pi f_{sw}} \times \frac{V_{p(peak)}}{I_{p(peak)}}; C \geq \frac{1}{(2\pi f_c)^2 L}. \tag{38}$$

where f_{sw} is a switching frequency, and $f_c = f_{sw}/10$.

Table 4. Parameters of a Multi-VSG Microgrid.

Para.	Values	Para.	Values	Para.	Value
P_1	15 kW	P_2	10 kW	P_3	7.5 kW
V_{ref}	380 V	V_{ref}	380 V	V_{ref}	380 V
ω	$2\pi \times 50$	f_{pwm}	5000 Hz	f_{pwm}	5000 Hz
f_n	50 Hz	f_n	50 Hz	f_n	50 Hz
$D_{(VSG-1)}$	40	$D_{(VSG-2)}$	40	$D_{(VSG-3)}$	40, 25, 15
R_1	0.05	R_2	0.05	R_3	0.05
L_1	1.45×10^{-3}	L_2	1.45×10^{-3}	L_3	1.45×10^{-3}
C_1	150×10^{-6}	C_2	150×10^{-6}	C_3	150×10^{-6}
V_{dc}	800 V	V_{dc}	800 V	V_{dc}	800 V
D_{q1}	0.010	D_{q2}	0.010	D_{q3}	0.010
J_1	0.1	J_2	0.1	J_3	0.1

5.1. Loading Analysis

The loading analysis is performed on four cases by adding 10 kW load to a multi-VSG island microgrid system. The case I, II and III have an equivalent droop control, whereas Case IV has a novel master–slave configuration of a VSG control. The power and angular frequency response of all sources are observed for each case.

5.1.1. Case I

The rated powers of VSG-1, VSG-2 and VSG-3 are 15 kW, 10 kW and 7.5 kW respectively, but the droop (damping) coefficient is the same ($D = 40$) for all VSG sources. As a result, the dynamic response of angular frequency is noticeably coordinated for all sources because of the same damping coefficient. The power is distributed on the basis of a droop control. VSG-1, VSG-2 and VSG-3 are sharing 72.8%, 59% and 45.2% of the total power rating respectively as shown in Figure 11 and in Table 5.

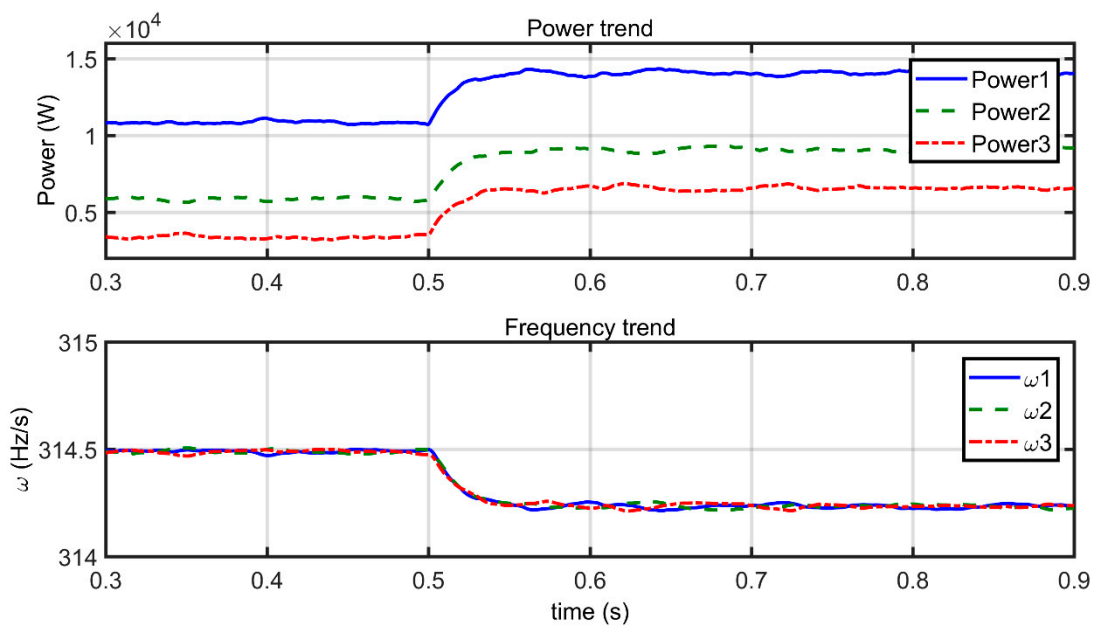


Figure 11. Power and Frequency Trend Case I.

Table 5. Parameters of a multi-VSG microgrid.

Cases	Condition	$\Delta\omega_a$	$\Delta\omega_b$	$\Delta\omega_c^o$	ω_o	P_1	P_2	P_3	$\%P_1^t$	$\%P_2^t$	$\%P_3^t$
Case I	$\omega_{nl}^1 > \omega_{nl}^2 > \omega_{nl}^3$	0.4	0.2	0.27	314.48	10.9	5.9	3.39	72.8	59	72.8
Case II	$\omega_{nl}^1 > \omega_{nl}^3 > \omega_{nl}^2$	0.24	0.16	0.42	314.53	10.3	5.27	4.55	68.7	52.7	68.7
Case III	$\omega_{nl}^3 > \omega_{nl}^1 > \omega_{nl}^2$	0.39	0.4	0.38	314.57	9.8	4.77	5.57	65.34	47.4	65.3
Case IV	$\omega_{nl}^3 = \omega_{fl}^3 = \omega$	0.4	-	-	314.65	8.75	3.75	7.5	58.3	37.5	100

When a droop coefficient is similar for different power rating sources, then the remaining power for all sources is equal. When two VSGs have a same active and reactive power rating, droop coefficient, inertia, and the reference frequency, then these VSGs are considered as ideally coordinated, as a result, the dynamic response of an angular frequency is exactly same and can be called as ‘reference dynamic response’. In this case, VSG-1 and VSG-2 have identical control parameters; except a power rating, but it can be observed in Figure 11 that the dynamic response is similar, so in our case, the angular frequency of VSG-1 and VSG-2 during dynamic state is a reference dynamic response of a system.

5.1.2. Case II

The power contribution of VSG-3 is increased by changing a droop coefficient to a smaller value at $D = 25$. The power percentage of VSG-3 is increased from 45.2% to 60.6% as shown in Figure 12. The drawback of reducing damping coefficient is the increases in a rate of change of angular frequency, as a result, the coordination of VSG-3 is slightly disturbed from other VSG sources.

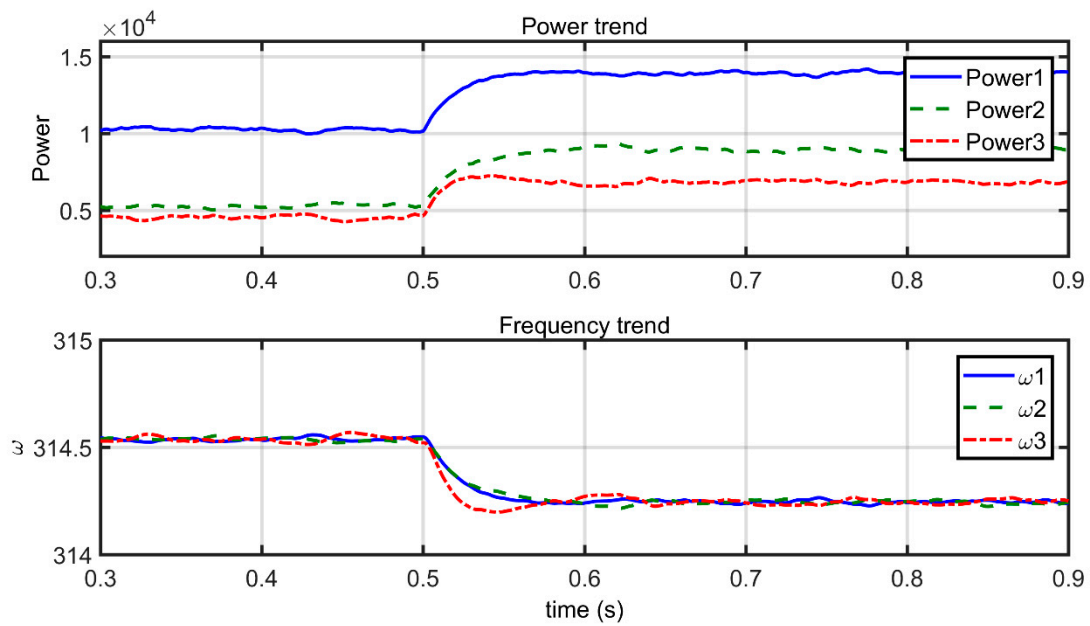


Figure 12. Power and Frequency Trend Case II.

5.1.3. Case III

The power contribution before adding a load is even more increased by changing a droop coefficient to $D = 15$. The percentage of VSG-3 power sharing is increased by 13% to 73.4%, whereas the power percentages of VSG-1 and VSG-2 are decreased to 65.34% and 47.7% respectively as shown in Figure 13. However, the angular frequency response of VSG-3 is deficient during the addition of a load due to low damping effect and high rate of change of frequency. The stabilizing time of power and angular frequency is also prolonged for VSG-3.

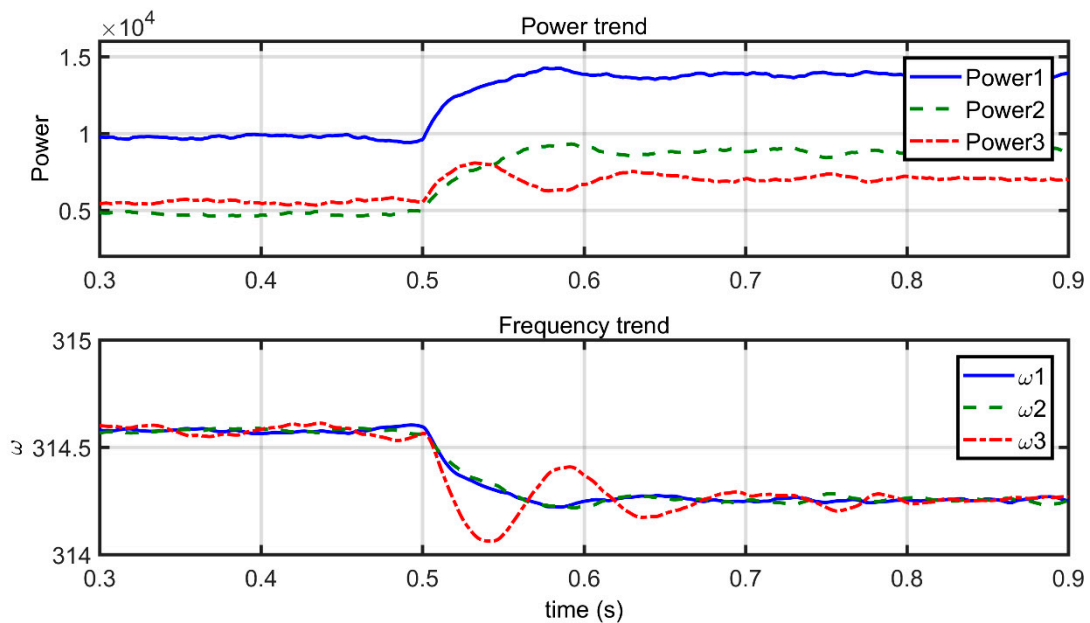


Figure 13. Power and Frequency Trend Case III.

5.1.4. Case IV

The simulation on a proposed master–slave VSG control is performed in this case. The reference angular frequency of VSG-3 is assumed to be a system’s operating angular frequency, consequently,

the reference power of VSG-3 is achieved by using a proposed control. The percentage of power delivered by VSG-3 is increased to 100% shown in Figure 14. A VSG-3 is getting back to its stable state after the addition of a load, though it is relatively slower than other sources. On the other hand, the coordinated of VSG-3 is mismatched to some extent with other VSG sources due to a higher rate of change of angular frequency. The angular frequency response of VSG-3 from a proposed control is better than Case III and nearly equal to Case II, but it is inferior to Case I.

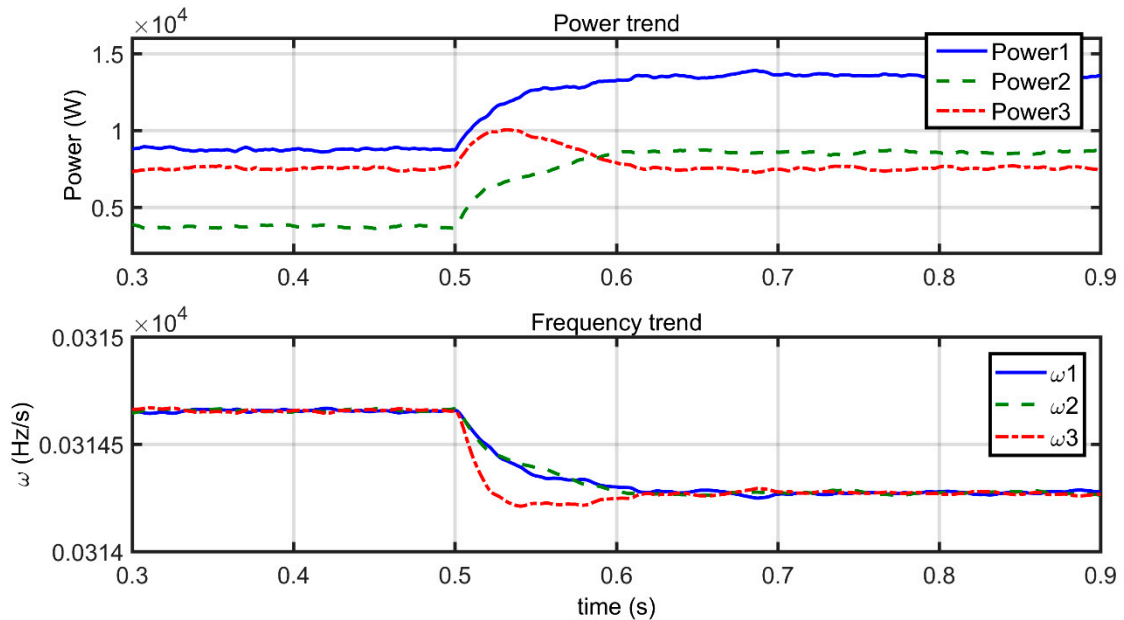


Figure 14. Power and Frequency Trend Case IV.

5.1.5. Comparison of Power of VSG-3

The comparison on a power delivered by VSG-3 from each Case is presented in Figure 15. When a droop coefficient ‘D’ of VSG-3 is 40 in Case I, then only 45.2% power is delivering to a load before the additional of a load. The power is increased to 60.6% and 73.4% in Case II and Case III respectively. A remarkable 100% power delivering is observed in Case IV.

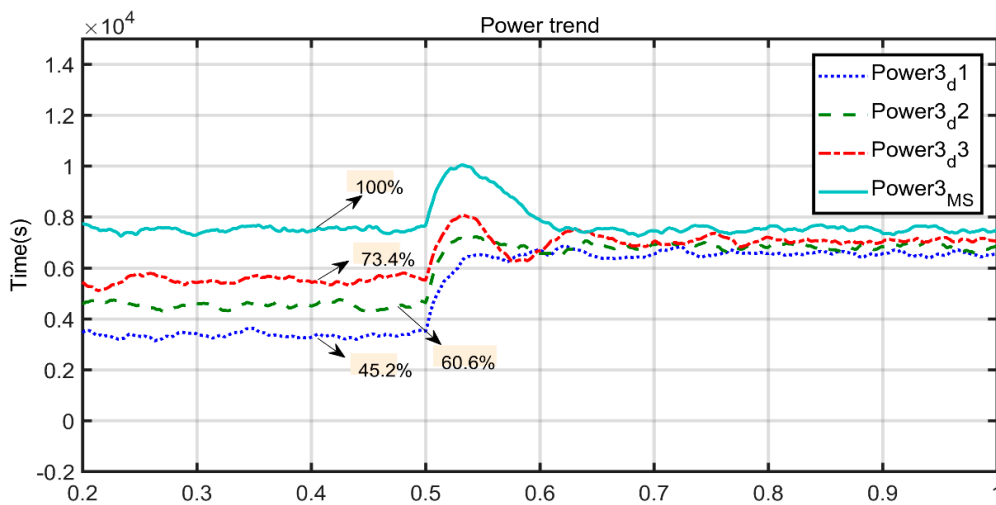


Figure 15. Power-delivered comparison.

5.1.6. Comparison of Angular Frequency (VSG-3)

The comparison on angular frequency for each case is executed to observe the response of a VSG-3 under the addition of a load or an abnormal condition. The static angular frequency of a system before the adding a load is different in each case due to the change in parameters of VSG-3 source. The angular frequency (before adding load) is at 314.48 Hz/s, 314.53 Hz/s, 314.57 Hz/s, and 314.65 Hz/s in Case I, II, III, and IV respectively as shown in Figure 16. The increase in a stable angular frequency is because of greater contribution of power from VSG-3. When a 10 kW load is added with a system, the response of angular frequency for each case is displayed in a figure. There is a significant difference in a static state of an angular frequency before load addition, whereas the difference is considerably decreased after the addition of a load; it is because a VSG-3 is operated nearly a rated power. The dynamic response of an angular frequency of Case I, Case II and Case IV is marginally different. However, the response of Case III is devastated and it has an irregular transition due to low damping coefficient and mismatching of VSG-3. The angular frequency of proposed control in case IV is showing a smoother response as compared to other cases.

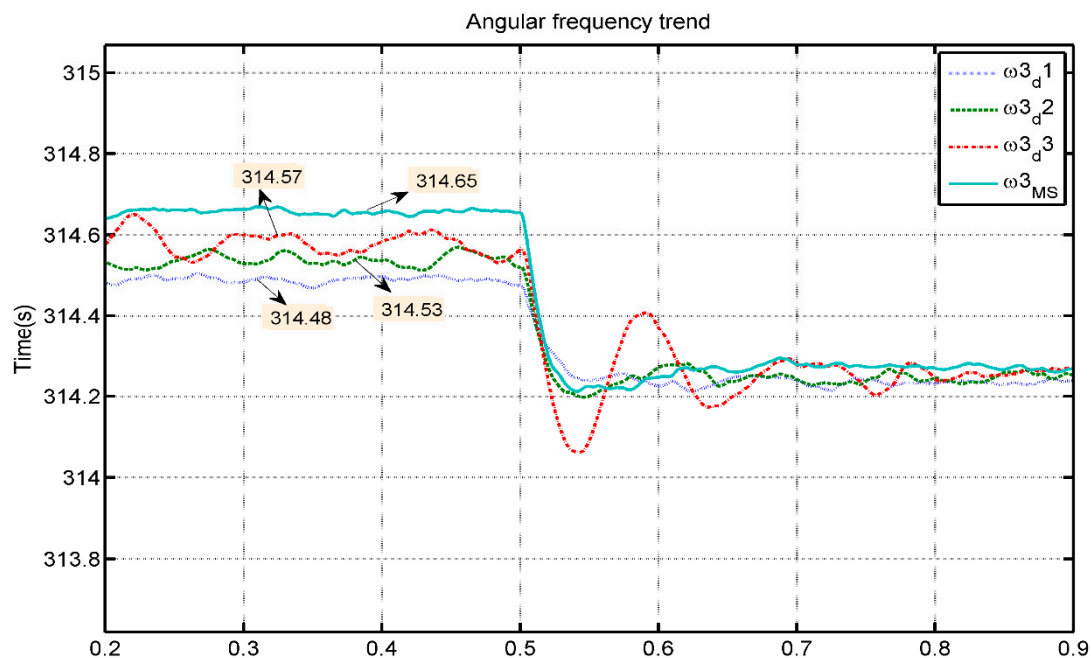


Figure 16. Comparison of angular frequency (VSG-3).

5.1.7. Rate of Change of Frequency Analysis

The rate of change of frequency of all sources for each case is observed to analyze the response of a VSG-3 source under different conditions in Figure 17. The identical values of RCF show a matching between the multiple VSG sources. The trend of RCF in Case I is similar for all sources, thus the coordination is strong. RCF of VSG-3 is slightly higher than VSG-1 and VSG-2 in Case II, so the coordination is little lower. The RCF of VSG-3 is deprived in Case III, consequently, it can be concluded that the coordinated of VSG-3 is not satisfactory.

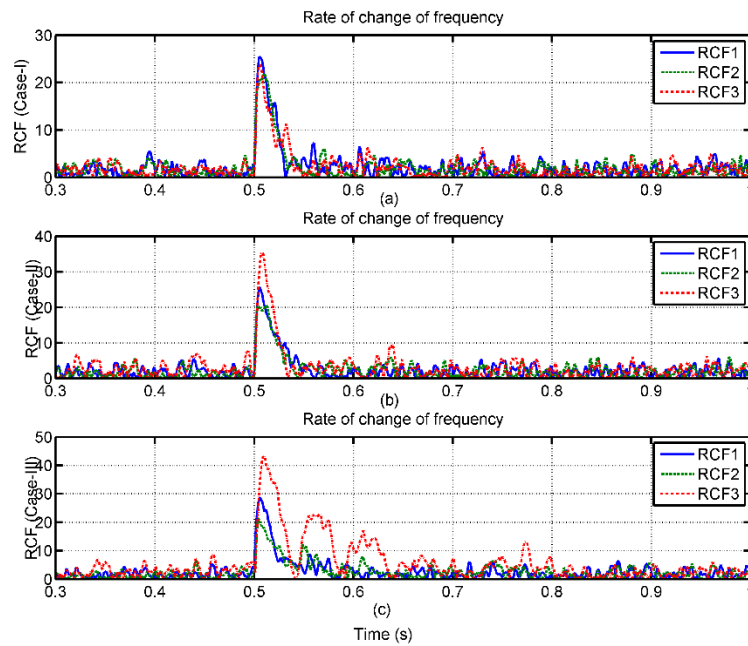


Figure 17. RCF analysis.

5.1.8. Comparison of RCF (VSG-3)

The RCF comparison of a VSG-3 of the four cases is displayed in Figure 18. The decrease in droop coefficient is causing an increase in RCF due to a decrease in a damping effect. It is to be noted that the RCF value of master–slave control is the highest, but the dynamic response of an angular frequency is almost similar and the stabilizing time is also satisfactory.

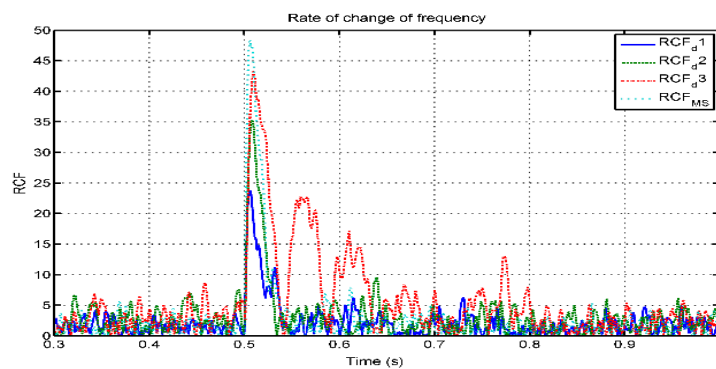


Figure 18. RCF comparison (VSG-3).

5.2. Fault Analysis

The fault analysis is performed to evaluate the behavior of VSG sources in a multiple-VSG system under a fault condition. The protection control is not introduced in any of VSG sources to investigate the dynamic behavior of sources. A three-phase to ground fault is applied near the load for 0.02 s at 1.0 s.

5.2.1. Case I

The dynamic response of power and angular frequency is identical under a fault is displayed in Figure 19. The angular frequency of VSG-1 is slightly higher than other sources because of the high power rating.

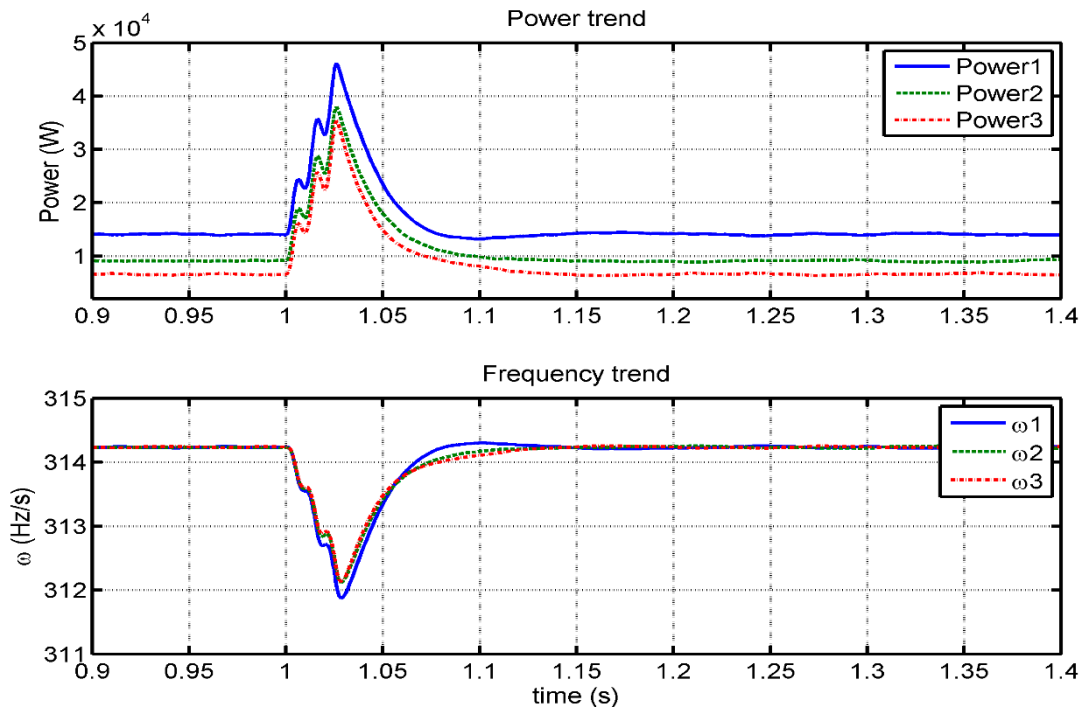


Figure 19. Fault Analysis Case I.

5.2.2. Case II

The response of VSG-3 is mismatched when a fault is applied in Case II is shown in Figure 20. The angular frequency is reached to a minimum level at 311.2 Hz/s that is 0.8 Hz/s less than the other sources and the stabilizing time of VSG-3 is slightly slower as compared with VSG-1 and VSG-2.

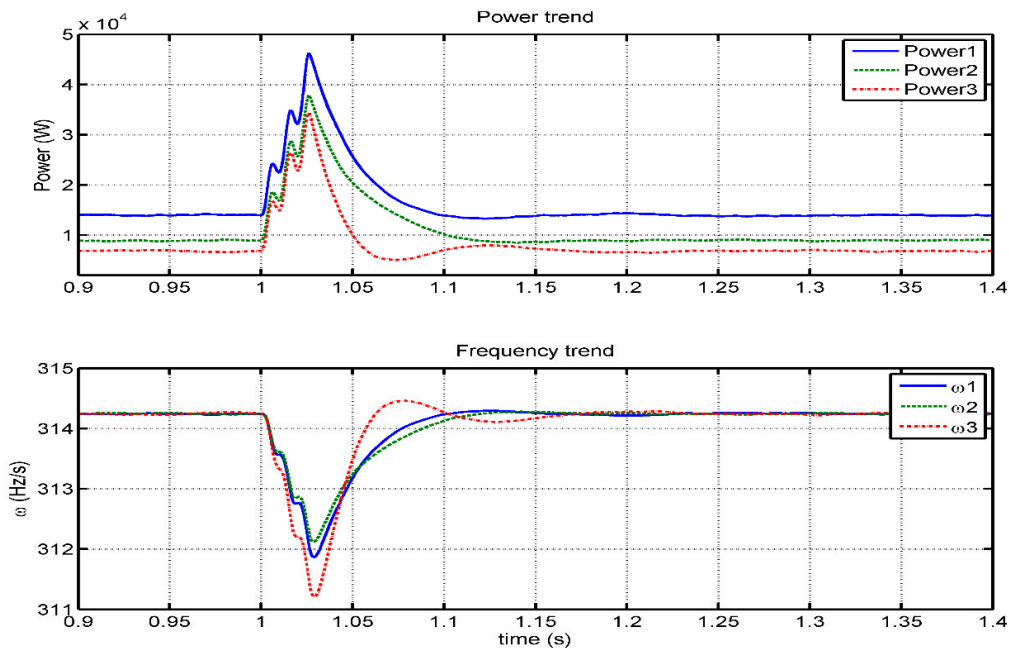


Figure 20. Fault Analysis Case II.

5.2.3. Case III

The oscillation in a power and angular frequency response of VSG-3 shows that it has an insufficient damping; the damping coefficient is small as shown in Figure 21.

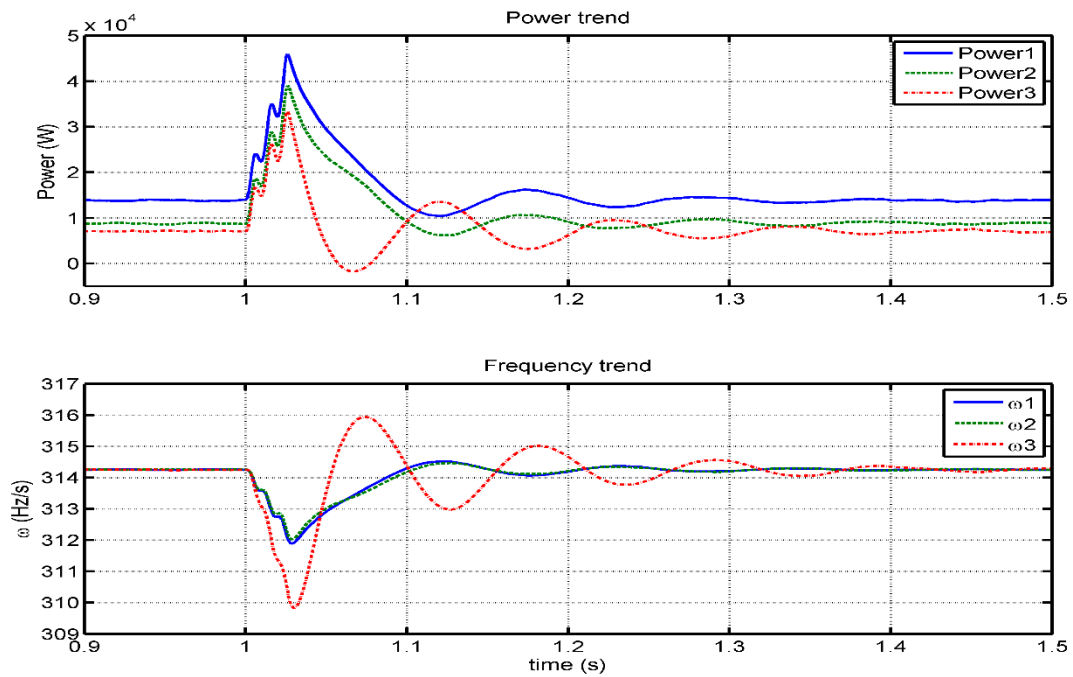


Figure 21. Fault Analysis Case III.

5.2.4. Case IV

The master–slave control is not showing oscillation; unlike Case III, and the stabilizing time almost the same with other VSG sources. The angular frequency is dropping down to 310 Hz/s that is 2 Hz/s lower than peer VSG sources in Case IV in Figure 22. Therefore, the improvement in a master–slave control is required to damp the instant effect of a fault.

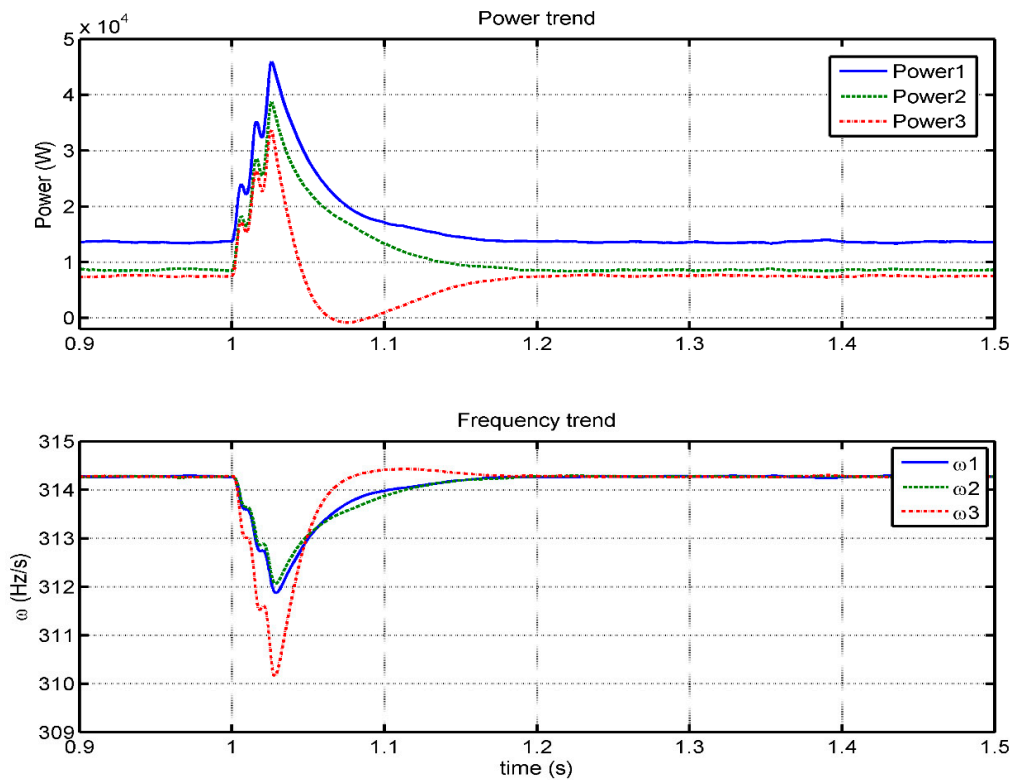


Figure 22. Fault Analysis Case IV.

5.2.5. Comparison of RCF Analysis Under Fault (VSG-3)

The rate of change of frequency (RCF) for all four cases of VSG-3 is compared to examine the change in the behavior of VSG-3 for different parameters and controls in Figure 23. The peak value of RCF is shown in a master-slave, whereas damping is quite faster in this case during a fault. On the contrary, the peak RCF of Case III is lower than the RCF of Case IV, but the stabilizing time is rather longer. The rate of change of frequency is reduced quickly and reaches to stable RCF limits in less time as compared to Case II and Case III, and almost equal to Case I (reference case).

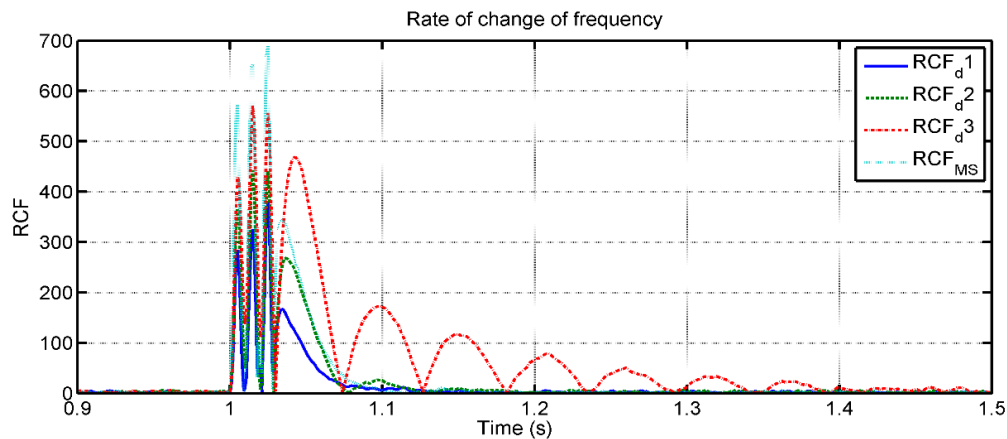


Figure 23. Comparison of RCF analysis under fault (VSG-3).

5.2.6. Comparison of Angular Frequency Under Fault (VSG-3)

The comparison of the angular frequency response of VSG-3 under fault for all cases is shown in Figure 24. The response of Case III is unstable after fault due to insufficient damping i.e., $D = 15$. The value of 'D' is set to lower value to increase a delivering power of VSG-3 to a system, but due to a dual characteristic of 'D' in the static and dynamic state as a droop coefficient and damping coefficient respectively, causing a low-damping effect of VSG-3. When a proposed master-slave VSG control is implemented by changing the reference angular frequency, then the delivering power is increased to its reference power, thus the angular frequency response is showing a better response than in Case IV. The angular frequency response of Case I is considered as a reference for the comparison, as the VSG source are coordinated by compromising a delivered power. The stabilizing time of a proposed MS-VSG control (Case IV) is almost the same as Case I and better than Case II and Case IV.

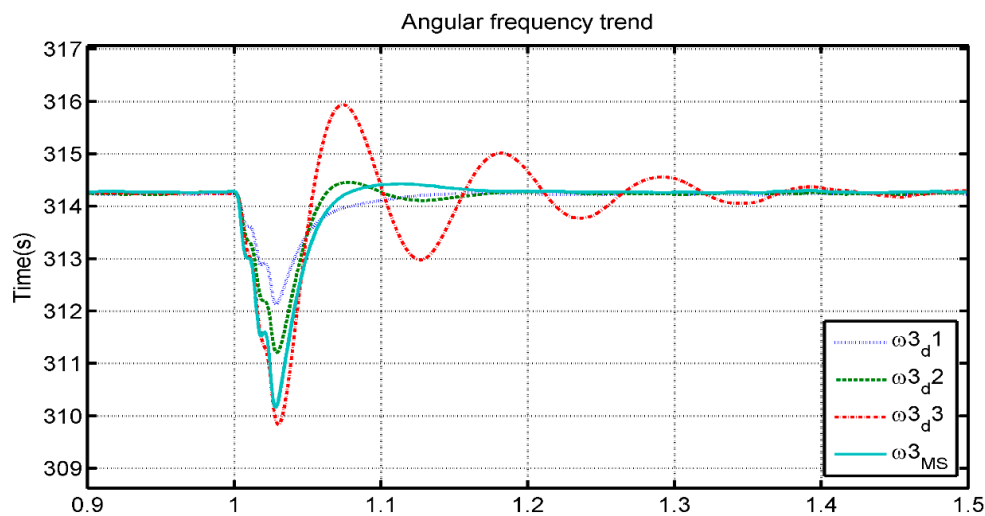


Figure 24. Comparison of angular frequency analysis under fault (VSG-3).

6. Discussion

Due to the high penetration of renewable energy source (RES) in a power system, the stability of a system is compromised due to the lack of reserved power and inertia. VSG control has inherent characteristics of droop and inertia control. However, there is a matching problem between multiple VSG sources. The power rating of different sources is not alike, so the same droop coefficient is not suitable for all source under a low-load condition. Secondly, the RES is an instant power generation and it is necessary to capture the maximum energy from it, otherwise, it goes in vain.

The analysis on multi-VSG sources system is performed by changing the parameters of one VSG source to evaluate the static and dynamic behavior of a system. It is observed that at a higher load, i.e., each source is delivering rated power to a system, the difference between delivered power from different droop coefficients is nearly the same. However, when the load is less, then the power sharing from VSG-3 is controlled by decreasing droop coefficient ' D ' of VSG-3. It is observed that the decrease in ' D ' is increasing the delivered power of VSG-3. A term ' D ' has dual characteristics i.e., droop coefficient and damping coefficient. A single parameter ' D ' is deciding the static state of a system by applying $P - \omega$ droop control ($D =$ droop coefficient), also it is providing a damping under an abnormal condition ($D =$ damping coefficient). When the power contribution of VSG-3 is increased by decreasing ' D ', the damping of VSG-3 is also degraded, as a result, the oscillation is causing throughout the results in all Cases other than Case I. The reason of oscillation is an inappropriate damping coefficient that in turn affecting the matching between VSG sources.

A master-slave control is introduced to operate a low power VSG source at a rated power. The advantage of this control is to provide 100% power to a load at any angular frequency of a system. Moreover, it is observed that the stabilizing time of VSG-3 from master-slave control is the same as compared with other VSG sources. However, there is one disadvantage of master-slave control, the rate of change in frequency of VSG-3 is the highest among all studies cases and the angular frequency drop is just better than Case III with droop coefficient of $D = 15$.

7. Conclusions

The static and a dynamic analysis of three sourced multi-VSG system is performed. The significance of the no-load frequency of each VSG source is considered to draw a load-sharing criteria. Three cases of droop controlled multi-VSG are established to derive the equations for calculating the total load sharing by each source and the operating angular frequency of multi-VSG system for any given load. The power sharing of VSG-3 is increased by the variation of a droop coefficient of $P - \omega$ droop control and by using a novel master-slave configuration of VSG control. The analysis results showed that the power sharing is increased by decreasing the droop coefficient ' D ', on the contrary, the stability of VSG-3 is compromised; it is because of the dual characteristic of ' D ' in a static (droop) and a dynamic (damping) state. The relationship of a damping coefficient ' D ' on a derivative of the change in frequency is derived and it showed that they are inversely proportional to each other. The master-slave configuration is showing a promising performance in terms of a power sharing i.e., 100% power is delivered from VSG-3, however, the angular frequency and a rate of change of frequency response during a dynamic condition are not encouraging. It is concluded that the droop coefficient of all sources in a multi-VSG system should be similar for a firm coordination, regardless of their power ratings. The performance of a master-slave configuration can be improved by implementing additional controls during transition in the future.

Author Contributions: Each author contributed extensively to the preparation of this manuscript. A.R. and X.Y. designed and developed the main research work, including designing the controller, and simulation model. A.R. and H.R. has worked on the analysis of the obtained results and writing original draft. H.G. and F.A. provided some useful suggestions in organizing research contents and the construction of a paper. All the authors revised and approved the publication.

Funding: This paper was supported by the Hebei Natural Science Funding (E2018502134); Liaoning Power Grid Corporation's 2018 Science and Technology Project "Research on the Reactive Power and Voltage Optimization Strategy and Evaluation Index Considering Source and Load Fluctuation Characteristics".

Acknowledgments: The author, A.R., would like to thank China Scholarship Council (CSC) for providing the funding during his PhD studies.

Conflicts of Interest: The authors declare no conflict of interest

References

1. Rasool, H.; Mutal, A.; Rasool, A.; Ahmad, W.; Ikram, A.A. MPPT based ASBC controller and solar panel monitoring system. In Proceedings of the 2014 International Conference on Energy Systems and Policies (ICESP), Islamabad, Pakistan, 24–26 November 2014; IEEE: Piscataway, NJ, USA, 2014.
2. Brabandere, K.D.; Bolsens, B.; Van den Keybus, J.; Woyte, A.; Driesen, J.; Belmans, R. A Voltage and Frequency Droop Control Method for Parallel Inverters. *IEEE Trans. Power Electron.* **2007**, *22*, 1107–1115. [[CrossRef](#)]
3. Chandorkar, M.C.; Divan, D.M.; Adapa, R. Control of parallel connected inverters in standalone AC supply systems. *IEEE Trans. Ind. Appl.* **1993**, *29*, 136–143. [[CrossRef](#)]
4. Nikkhajoei, H.; Lasseter, R.H. Distributed Generation Interface to the CERTS Microgrid. *IEEE Trans. Power Deliv.* **2009**, *24*, 1598–1608. [[CrossRef](#)]
5. Vandoorn, T.L.; Meersman, B.; De Kooning, J.D.; Vandeveld, L. Analogy between conventional grid control and islanded microgrid control based on a global DC-link voltage droop. *IEEE Trans. Power Deliv.* **2012**, *27*, 1405–1414. [[CrossRef](#)]
6. Hashmi, K.; Mansoor Khan, M.; Jiang, H.; Umair Shahid, M.; Habib, S.; Talib Faiz, M.; Tang, H. A Virtual Micro-Islanding-Based Control Paradigm for Renewable Microgrids. *Electronics* **2018**, *7*, 105. [[CrossRef](#)]
7. Driesen, J.; Visscher, K. Virtual synchronous generators. In Proceedings of the 2008 IEEE Power and Energy Society General Meeting—Conversion and Delivery of Electrical Energy in the 21st Century, Pittsburgh, PA, USA, 20–24 July 2008.
8. Hirase, Y.; Noro, O.; Yoshimura, E.; Nakagawa, H.; Sakimoto, K.; Shindo, Y. Virtual synchronous generator control with double decoupled synchronous reference frame for single-phase inverter. *IEEJ J. Ind. Appl.* **2015**, *4*, 143–151. [[CrossRef](#)]
9. Chen, Y.; Hesse, R.; Turschner, D.; Beck, H.P. Improving the grid power quality using virtual synchronous machines. In Proceedings of the 2011 International Conference on Power engineering, energy and electrical drives (POWERENG), Malaga, Spain, 11–13 May 2011; IEEE: Piscataway, NJ, USA, 2011.
10. Beck, H.-P.; Hesse, R. Virtual synchronous machine. In Proceedings of the 9th International Conference on Electrical Power Quality and Utilisation, EPQU 2007, Barcelona, Spain, 9–11 October 2007; IEEE: Piscataway, NJ, USA, 2007.
11. Zhong, Q.-C.; Weiss, G. Synchronverters: Inverters that mimic synchronous generators. *IEEE Trans. Ind. Electron.* **2011**, *58*, 1259–1267. [[CrossRef](#)]
12. Liu, J.; Miura, Y.; Bevrani, H.; Ise, T. Enhanced Virtual Synchronous Generator Control for Parallel Inverters in Microgrids. *IEEE Trans. Smart Grid* **2016**, *8*, 2268–2277. [[CrossRef](#)]
13. Hirase, Y.; Noro, O.; Nakagawa, H.; Yoshimura, E.; Katsura, S.; Abe, K.; Sugimoto, K.; Sakimoto, K. Decentralised and interlink-less power interchange among residences in microgrids using virtual synchronous generator control. *Appl. Energy* **2018**, *228*, 2437–2447. [[CrossRef](#)]
14. Cao, Y.; Wang, W.; Li, Y.; Tan, Y.; Chen, C.; He, L.; Häger, U.; Rehtanz, C. A Virtual Synchronous Generator Control Strategy for VSC-MTDC Systems. *IEEE Trans. Energy Convers.* **2018**, *33*, 750–761. [[CrossRef](#)]
15. Wang, F.; Zhang, L.; Feng, X.; Guo, H. An Adaptive Control Strategy for Virtual Synchronous Generator. *IEEE Trans. Ind. Appl.* **2018**, *54*, 5124–5133. [[CrossRef](#)]
16. Ma, Y.; Lin, Z.; Yu, R.; Zhao, S. Research on Improved VSG Control Algorithm Based on Capacity-Limited Energy Storage System. *Energies* **2018**, *11*, 677. [[CrossRef](#)]
17. Alipoor, J.; Miura, Y.; Ise, T. Power System Stabilization Using Virtual Synchronous Generator With Alternating Moment of Inertia. *IEEE J. Emerg. Sel. Top. Power Electron.* **2015**, *3*, 451–458. [[CrossRef](#)]
18. Shintai, T.; Miura, Y.; Ise, T. Oscillation Damping of a Distributed Generator Using a Virtual Synchronous Generator. *IEEE Trans. Power Deliv.* **2014**, *29*, 668–676. [[CrossRef](#)]

19. Cheng, C.; Zeng, Z.; Yang, H.; Zhao, R. Wireless parallel control of three-phase inverters based on virtual synchronous generator theory. In Proceedings of the International Conference on Electrical Machines and Systems, Busan, South Korea, 26–29 October 2013.
20. Paquette, A.D.; Reno, M.J.; Harley, R.G.; Divan, D.M. Sharing Transient Loads: Causes of Unequal Transient Load Sharing in Islanded Microgrid Operation. *IEEE Ind. Appl. Mag.* **2014**, *20*, 23–34. [[CrossRef](#)]
21. Rasool, A.; Yan, X.; Rasool, H.; Guo, H.; Asif, M. VSG Stability and Coordination Enhancement under Emergency Condition. *Electronics* **2018**, *7*, 202. [[CrossRef](#)]
22. Aazim, R.; Liu, C.; Haaris, R.; Mansoor, A. Rapid generation of control parameters of Multi-Infeed system through online simulation. *Ingeniería e Investigación* **2017**, *37*, 67–73. [[CrossRef](#)]
23. Banu, I.V.; Istrate, M. Islanding Prevention Scheme for Grid-Connected Photovoltaic Systems in Matlab/Simulink. In Proceedings of the 2014 49th International Universities Power Engineering Conference (UPEC), Cluj-Napoca, Romania, 2–5 September 2014; IEEE: Piscataway, NJ, USA, 2014.
24. Alipoor, J.; Miura, Y.; Ise, T. Stability assessment and optimization methods for microgrid with multiple VSG units. *IEEE Trans. Smart Grid* **2018**, *9*, 1462–1471. [[CrossRef](#)]
25. Chen, L.; He, H.; Zhu, L.; Guo, F.; Shu, Z.; Shu, X.; Yang, J. Coordinated control of SFCL and SMES for transient performance improvement of microgrid with multiple DG units. *Can. J. Electr. Comput. Eng.* **2016**, *39*, 158–167. [[CrossRef](#)]
26. Yu, B. An Improved Frequency Measurement Method from the Digital PLL Structure for Single-Phase Grid-Connected PV Applications. *Electronics* **2018**, *7*, 150. [[CrossRef](#)]



© 2018 by the authors. Licensee MDPI, Basel, Switzerland. This article is an open access article distributed under the terms and conditions of the Creative Commons Attribution (CC BY) license (<http://creativecommons.org/licenses/by/4.0/>).